# Supporting information for:

# Thermal Conductivity and Phonon Transport in Suspended Few-Layer Hexagonal Boron Nitride

*Insun Jo[1], Michael Thompson Pettes[2], Jaehyun Kim[2], Kenji Watanabe[3], Takashi Taniguchi[3], and Zhen Yao[1], Li Shi[2]*

[1]Department of Physics and [2]Department of Mechanical Engineering, The University of Texas at Austin, Austin, TX 78712, USA

[3]National Institute for Materials Science (NIMS), Tsukuba, Ibaraki 305-0044, Japan

* Corresponding author. E-mail: lishi@mail.utexas.edu

1. Optical, Atomic Force Microscopy (AFM), and Transmission Electron Microscopy (TEM) Images of h-BN Samples
2. Thermal Conductivity Calculation
3. Contact Thermal Resistance and Interface Conductance

1. Optical, Atomic Force Microscopy (AFM), Transmission Electron Microscopy (TEM) Images of h-BN Samples

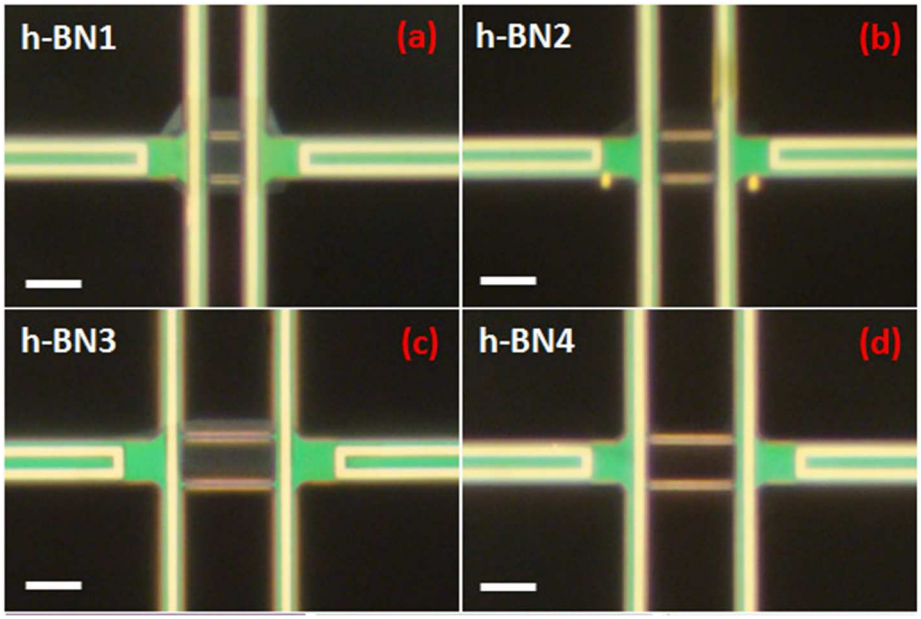


**Figure S1.** (a-d) Optical images of suspended h-BN after thermal annealing. The thicknesses of h-BN1–4 are determined to be 12±1, 12, 11, and 5 layers, respectively. Due to optical transparency in thin layer h-BN, h-BN4 is almost invisible under an optical microscope, although thicker h-BN1–3 can be seen clearly. The scale bars indicate 5 μm.

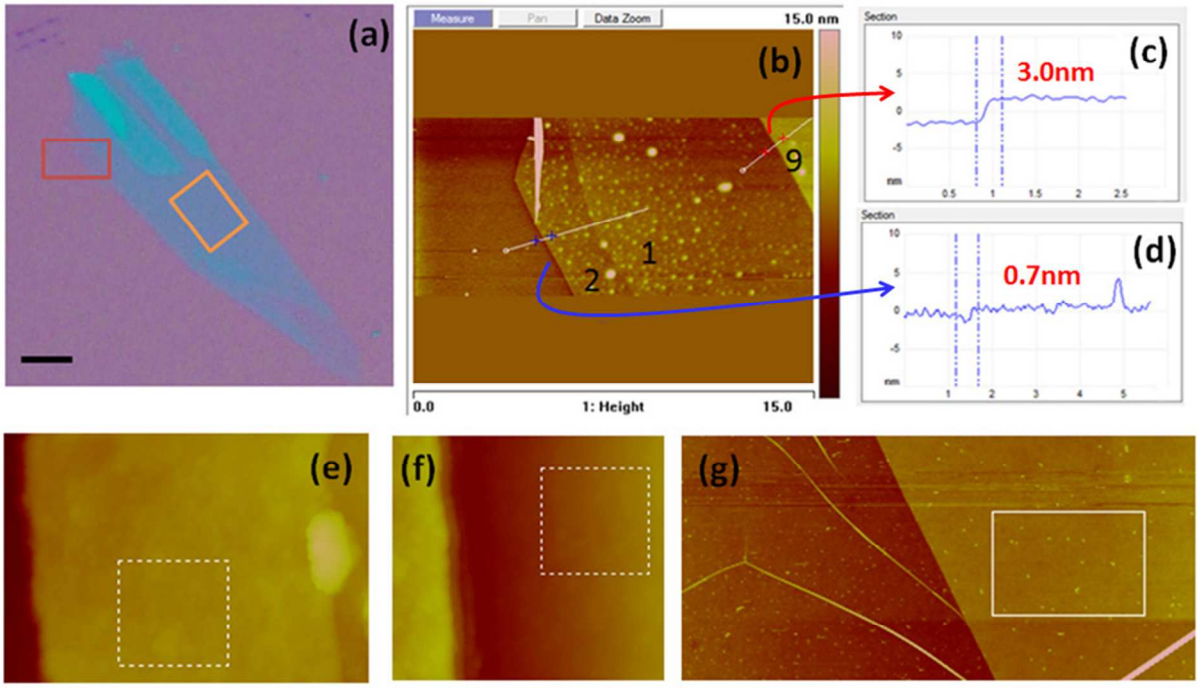


**Figure S2.** Optical image of h-BN1 showing the area scanned by atomic force microscopy (AFM) (red rectangle) and the area patterned and transferred (orange rectangle) to the suspended device in Fig. S1(a). The scale bar is 10 μm. (b) AFM topography of h-BN1 with discrete layer steps near the edge, with each step equal to 0.33 nm. The numbers in (b) indicate the change in layer thicknesses that were identified from the section analysis in AFM as shown in (c) and (d), where the numbers are the measured step height. The surface roughness of the (e) Pt thermometer and (f) $SiN_x$ beam of the micro-bridge device were measured to be 1.1 and 0.45 nm, respectively. (g) The roughness of an exfoliated 9 layer h-BN after annealing was measured to be 0.16 nm.

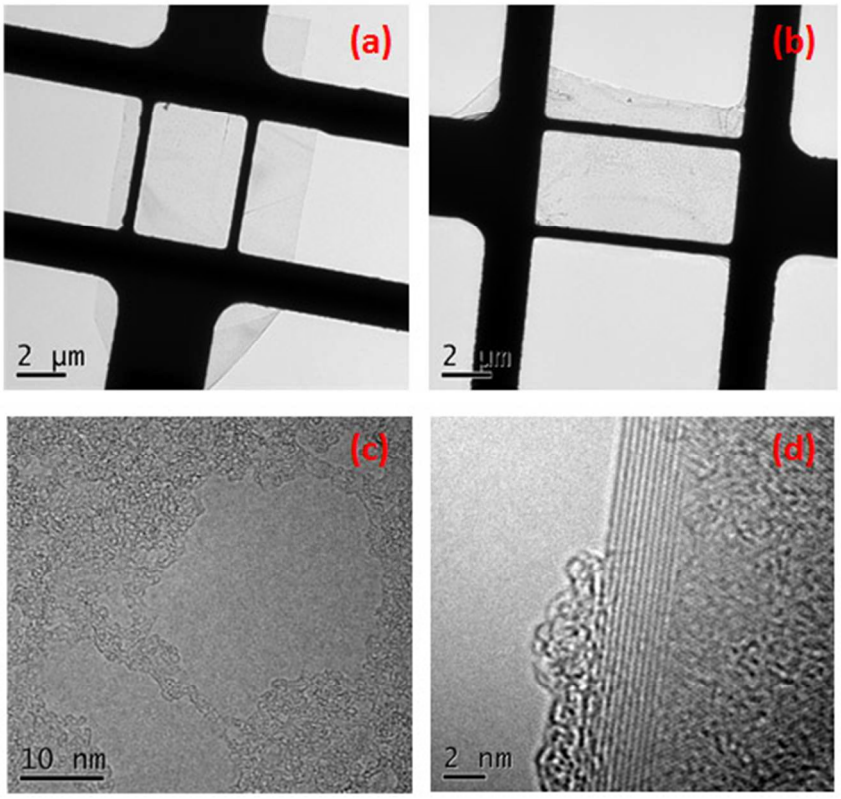


**Figure S3.** Low magnification TEM images of suspended (a) h-BN2 and (b) h-BN4. (c) Polymer residues observed over a large area of h-BN1. (d) The number of layers in h-BN3 can be observed by counting the (0002) fringes at the edge of the suspended section.

## 2. Thermal Conductivity Calculation

We used Quantum Espresso, an *ab initio* package, to calculate the phonon dispersion of h-BN. The unit cell parameters for h-BN used in the calculation are $a$ = 0.2479 nm and $c$ = 0.6998 nm.[1-3] The unit cell thickness is $c$ for bulk and multi- layer h-BN, and $c/2$ = 0.3499 nm for single layer h-BN. In the calculation, core-electrons were replaced by a pseudo-potential and valence electrons are described by a number of plane waves with an energy cutoff 70 a.u. in the self-consistent calculation. The calculation was performed on an 8×8×4 k-point grid in the Brillouin zone, while coarse $c$-axis grid resulted in divergence of the soft ZA and ZO' modes.

The dynamical matrix was calculated on a 5×5×4 grid in k-space, followed by interatomic force constant calculation in real space. The calculated phonon dispersion results for bulk h-BN are shown in Fig. S4, and in agreement with literature experimental data obtained from inelastic X-ray scattering,[3] Raman spectroscopy,[4-6] and Infrared spectroscopy.[4] The interlayer coupling in multi-layer h-BN results in the splitting of the low-frequency phonons near the Γ point, and gives rise to three low-energy optical branches, namely the ZO', LO', TO' branches. For few-layer h-BN, we considered the 6 lowest-energy phonon branches in the thermal conductivity calculation based on Eq. (1) of the main text. Both the polarization-specific phonon group velocity, $v_p$, and the density of states, $D_p(\omega)$, were calculated from the phonon dispersion in the basal plane, which was assumed to be isotropic and the same as that found along the Γ–M direction.

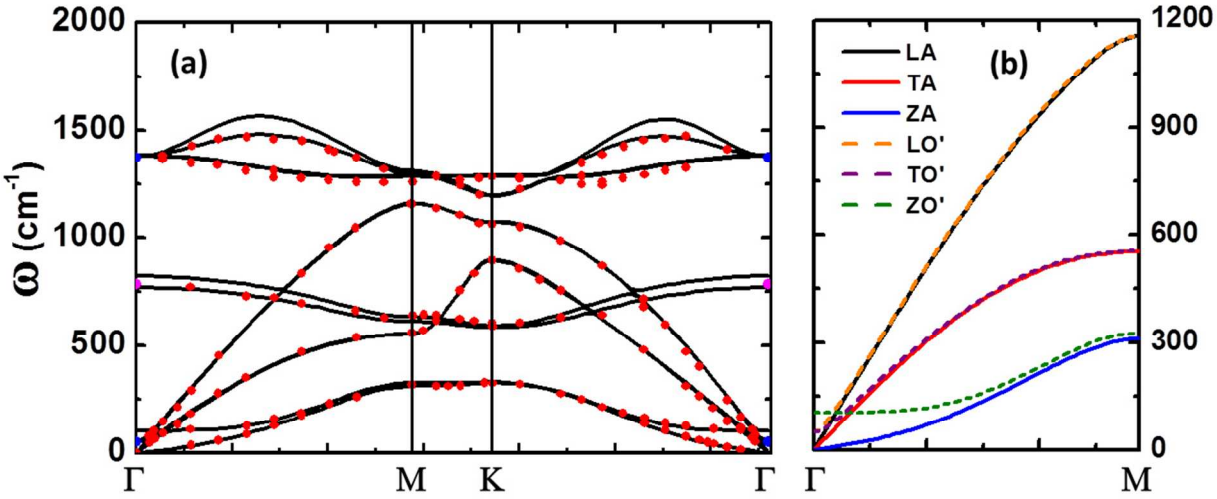


**Figure S4.** Phonon dispersion of (a) bulk h-BN (b) low-energy phonon branches used for thermal conductivity calculation. Reported measurement data from inelastic X-ray scattering (red circle),[3] Raman spectroscopy (blue circle),[4-6] and Infrared spectroscopy[4] (magenta circle) are also shown in (a).

Three types of phonon scattering mechanisms are considered in the calculation. The synthesized h-BN consists of 19.9% $^{10}$B and 80.1% $^{11}$B, whereas the isotopic variance of N is negligible. Phonon scattering by isotopic impurities is calculated as[7]

$$\tau_{D,p}^{-1} = \frac{S_0 \Gamma}{4} \frac{k_p}{v_p} \omega_p^2 \quad \text{(S1)}$$

where $S_0$ is the cross-sectional area per atom and $\Gamma$ is the strength of the point defect scattering, which is obtained as $\Gamma = \sum_i f_i (1 - M_i / \overline{M})^2 = 0.00136$,[8] where $f_i$ is the fractional concentration of the impurity atoms, $M_i$ is the mass of the impurity, and $\overline{M}$ is the average atomic mass of boron.

Phonon scattering by other point defects such as vacancies and impurities are also calculated from Eq. (S1). The phonon scattering rate by the lateral edges of the few-layer h-BN sample is calculated as $\tau_{B,p}^{-1} = v_p / l_b$, where $l_b$ is the boundary scattering mean free path. Matthiessen's rule was used to account for the combined effects of different scattering mechanisms.

Figure S5 shows the calculation results for different $l_b$ values and different point defect concentrations. The calculation does not account for phonon scattering by polymer residues and Umklapp scattering, the latter of which is expected to be negligible at the low temperature limit. Because of the high isotopic impurity concentration, the calculation shows that isotope impurity scattering dominates over scattering by point vacancies at a concentration as high as $10^{20}$ cm$^{-3}$. An $l_b$ value of 2 μm can be used to fit the low-temperature experimental thermal conductivity values for bulk h-BN.[8] In comparison, without accounting for scattering by polymer residues, the $l_b$ value needs to be as small as 550 nm and 180 nm in order to match the experimental thermal conductivity data for the 11-layer and 5-layer sample, respectively. These $l_b$ values are much

smaller than the smallest geometrical boundary length of 3 μm of the single crystalline few-layer h-BN flakes.

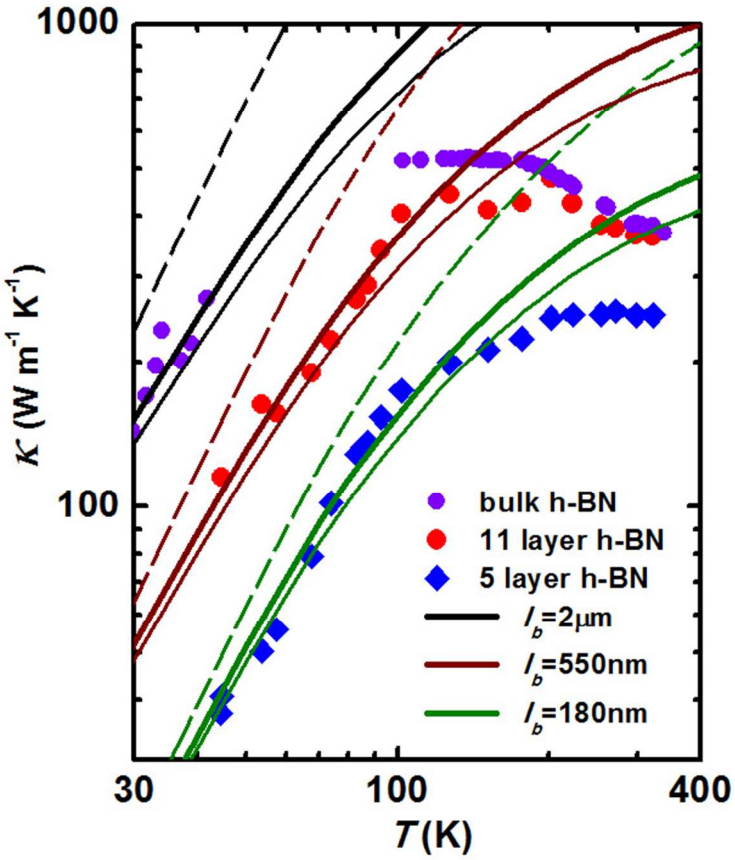


**Figure S5.** Comparison between the experimental thermal conductivity and calculation results for different $l_b$ values with no isotope impurities or point vacancies (thin dashed curves), with 19.9% $^{10}$B and 80.1% $^{11}$B and no point vacancies (thick solid curves), and with 19.9% $^{10}$B and 80.1% $^{11}$B and point vacancy concentration $n_D = 10^{20}$ cm$^{-3}$ (thin solid curves). Phonon scattering by polymer residues and Umklapp scattering are not included in the calculation.

## 3. Contact Thermal Resistance and Interface Conductance

We have evaluated the thermal contact thermal resistance and thermal interface conductance between the h-BN sample and the micro-bridge device using two different models. Figure S6 shows a scanning electron microscopy (SEM) image of h-BN1 and a schematic that defines the sample dimensions including the dimensions of the contact areas. While the contact length ($L_c$) between the sample and the straight resistance thermometer is the same among the samples, the contact lengths ($L_{c1}$ and $L_{c2}$) between the sample and the two U-shaped lines vary, as shown in Table S1. In the first contact thermal resistance model based on the linear fitting approach, the contact area between the h-BN and the two U-shaped lines is ignored. On the basis of this assumption, the less than 33% contribution from the contact thermal resistance suggests that the temperature difference between the h-BN and the underlying support should have decreased exponentially to be negligible as the h-BN extends onto U-shaped lines. This assumption would yield the same $R_cW$ values for different samples provided that the interface thermal conductance ($g_i$) per unit contact area is the same among the samples. In this model, the lateral temperature distribution at the contact area is treated by a fin heat transfer model to obtain the contact thermal resistance according to[9, 10]

$$R_c^{-1} = \sqrt{\kappa_s A w g_i}\,\tanh\left(L_c\sqrt{\frac{g_i}{\kappa_s t}}\right) \tag{S2}$$

where $\kappa_s$ is the thermal conductivity of the supported few-layer h-BN, $g_i$ is the thermal interface conductance per unit area, and $A$ and $w$ are the cross section and width of the few-layer h-BN sample. Because of additional phonon scattering by the interface between the h-BN and the micro-device, the thermal conductivity of the supported h-BN can be lower than that for the

suspended h-BN, as shown by recent measurements in supported graphene[11, 12] and encased graphene.[13] Nevertheless, the difference is expected to decrease with increasing layer thickness. Moreover, it has been found that the thermal conductivity of polymer-contaminated suspended bi-layer graphene[14] is similar to that of supported bi-layer graphene.[15] For the polymer-contaminated, 11-layer h-BN sample where the room-temperature thermal conductivity of the suspended region is found to approach that for bulk h-BN, we assume that $\kappa_s$ is the same as the thermal conductivity obtained for the suspended segment and use the obtained $R_c$ from linear fitting and Eq. (S2) to determine the interface conductance $g_i$.

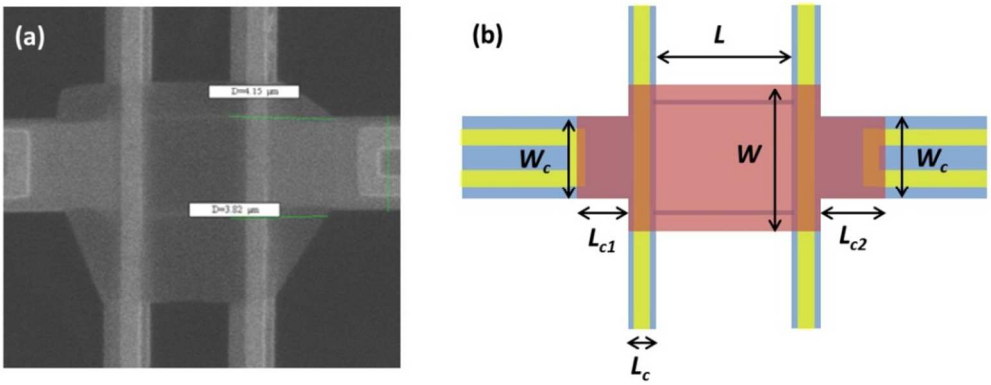


**Figure S6.** (a) Scanning electron micrograph of h-BN1. (b) Definitions of the dimension used in the contact thermal resistance models. The extended lengths $L_{c1}$ and $L_{c2}$ are measured for each sample and shown in Table S1. $W_c$ =3.8 μm is the same for all devices.

**Table S1.** The measured contact lengths of the extended region of h-BN samples.

| | h-BN1 | h-BN2 | h-BN3 | h-BN4 |
|---|---|---|---|---|
| $L_{c1}$ (μm) | 1.8 | 3.1 | 6.5 | 4.7 |
| $L_{c2}$ (μm) | 2.3 | 1.8 | 6.9 | 11.7 |

In the second contact thermal resistance model, we consider interface heat transfer in both regions of the contact area, including (1) the contact area between the sample and the two straight thermometer lines with a contact length $L_c$ = 1.7 μm, and (2) the extended h-BN area covering the part of the U-shaped lines with a width of $W_c$ = 3.8 μm. We have derived an expression of the total measured thermal resistance of the h-BN sample as

$$R_s(g_i,k)=\frac{L}{k\ t\ w}+\sum_{x=1}^{2}\frac{1}{M\left[\coth mL_c-\dfrac{1}{\sinh mL_c\cosh mL_c-\dfrac{w_c}{w}\sinh^2 mL_c\tanh mL_{cx}}\right]} \qquad \text{(S3)}$$

where the difference between the thermal conductivities ($\kappa$) of the suspended and supported h-BN regions have been ignored. The definitions of $m=\sqrt{\frac{g_i}{\kappa\ t}}$ , $M=w\sqrt{kg_it}$ , where $t$ is the sample thickness, are used according to the standard heat transfer model for extended surfaces or fins.[16] Based on Eq. (S3), we first find the different ($g_i$ , $\kappa$) data sets that would yield the measured thermal resistance of the 7.5 μm-long, 11 layer-thick h-BN3 sample at each temperature. From these different data sets, we find the ($g_i$ , $\kappa$) values that can best fit the measurement data of h-BN1 and h-BN2 with Eq. (S3) by minimizing the square root of the sum

of the squares of the relative error. The as-obtained $\kappa$ and $g_i$ values at different temperatures are shown in Figs. S7 (a) and (b), respectively, together with the values obtained from the first model based on linear fitting.

The difference in the $\kappa$ values obtained from the two models range between 3-36 % for the 11-layer sample and between 1-7 % for 5-layer sample. It is apparent from these results that the two models yield the same conclusion regarding the thickness dependence of the thermal conductivity of the few-layer h-BN. In addition, the obtained $g_i$ is about 1–2 orders of magnitude lower than that measured for supported few-layer graphene.[17] The low $g_i$ value for the h-BN sample can be caused by organic contamination left at the interface during the transfer process as well as the surface roughness of the micro-bride device.

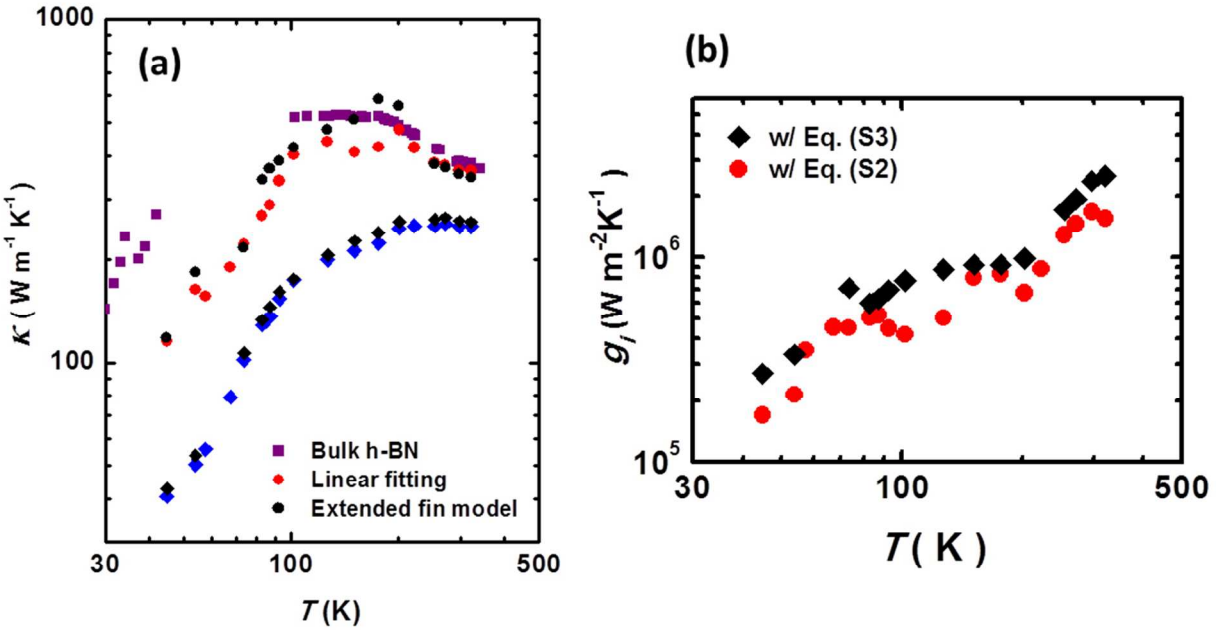

**Figure S7**. (a) Thermal conductivity values of few-layer h-BN samples obtained by two different contact thermal resistance models, namely the linear fitting approach and the extended fin model, together with the reported bulk h-BN values.[18] The red and black symbols are data from the linear fitting and the extended fin model, respectively. Squares, circles, and diamonds correspond to the bulk, 11-layer, and 5-layer h-BN samples, respectively. (b) Interface thermal conductance values obtained from the two contact thermal resistance models.

Supporting References.


1. Karch, K.; Bechstedt, F., *Phys Rev B* **1997,** *56*, 7404-7415.
2. Kern, G.; Kresse, G.; Hafner, J., *Phys Rev B* **1999,** *59*, 8551-8559.
3. Serrano, J.; Bosak, A.; Arenal, R.; Krisch, M.; Watanabe, K.; Taniguchi, T.; Kanda, H.; Rubio, A.; Wirtz, L., *Phys Rev Lett* **2007,** *98*, 095503.
4. Geick, R.; Perry, C. H.; Rupprech.G, *Phys Rev* **1966,** *146*, 543.
5. Nemanich, R. J.; Solin, S. A.; Martin, R. M., *Phys Rev B* **1981,** *23*, 6348-6356.
6. Reich, S.; Ferrari, A. C.; Arenal, R.; Loiseau, A.; Bello, I.; Robertson, J., *Phys Rev B* **2005,** *71*, 205201.
7. Nika, D. L.; Pokatilov, E. P.; Askerov, A. S.; Balandin, A. A., *Phys Rev B* **2009,** *79*, 155413.
8. Lindsay, L.; Broido, D. A., *Phys Rev B* **2011,** *84*, 155421.
9. Pettes, M. T.; Shi, L., *Adv Funct Mater* **2009,** *19*, 3918-3925.
10. Yu, C. H.; Saha, S.; Zhou, J. H.; Shi, L.; Cassell, A. M.; Cruden, B. A.; Ngo, Q.; Li, J., *J Heat Trans-T Asme* **2006,** *128*, 234-239.
11. Cai, W. W.; Moore, A. L.; Zhu, Y. W.; Li, X. S.; Chen, S. S.; Shi, L.; Ruoff, R. S., *Nano Lett* **2010,** *10*, 1645-1651.
12. Seol, J. H.; Jo, I.; Moore, A. L.; Lindsay, L.; Aitken, Z. H.; Pettes, M. T.; Li, X. S.; Yao, Z.; Huang, R.; Broido, D.; Mingo, N.; Ruoff, R. S.; Shi, L., *Science* **2010,** *328*, 213-216.
13. Jang, W. Y.; Chen, Z.; Bao, W. Z.; Lau, C. N.; Dames, C., *Nano Lett* **2010,** *10*, 3909-3913.
14. Pettes, M. T.; Jo, I. S.; Yao, Z.; Shi, L., *Nano Lett* **2011,** *11*, 1195-1200.

15. Sadeghi, M. M.; Shi, L., *Proceedings of the ASME 2011 International Mechanical Engineering Congress & Exposition* **2011,** *IMECE2011-64227*.

16. Incropera, F.; DeWitt, D., *Fundmentals of heat and mass transfer, pp. 133, Wiley* **2002**.

17. Mak, K. F.; Lui, C. H.; Heinz, T. F., *Appl Phys Lett* **2010,** *97*, 221904.

18. Sichel, E. K.; Miller, R. E.; Abrahams, M. S.; Buiocchi, C. J., *Phys Rev B* **1976,** *13*, 4607-4611.